Review of focused ion beam implantation mixing for the fabrication of GaAs-based optoelectronic devices

A. J. Steckl[a] and P. Chen
Department of Electrical and Computer Engineering, University of Cincinnati, Cincinnati, Ohio 45221-0030

H. E. Jackson, A. G. Choo, and X. Cao
Department of Physics, University of Cincinnati, Cincinnati, Ohio 45221-0011

J. T. Boyd and M. Kumar
Department of Electrical and Computer Engineering, University of Cincinnati, Cincinnati, Ohio 45221-0030

(Received 19 July 1995; accepted 24 August 1995)

The fabrication of GaAs-based optoelectronic components by the technique of focused ion beam (FIB) implantation mixing is reviewed. The basic mechanisms and practice of the FIB-induced mixing process of GaAs/AlGaAs multiple quantum well and superlattice structures are discussed. The use of the FIB mixing technique for the fabrication of optoelectronic devices (such as channel waveguides and distributed Bragg reflection distributed feedback lasers) by the single-step, maskless/resistless FIB implantation process is described and their characteristics are reviewed. © *1995 American Vacuum Society.*

I. INTRODUCTION

Great progress has been made in recent years in the development of photonic integrated circuits (PICs) and optoelectronic integrated circuits (OEICs). One source limiting the expansion of OEIC capability has been the complexity required for fabrication using conventional technology (in particular lithography, etching, and implantation), which has to satisfy various requirements for different components fabricated on the same substrate.[1] An interesting alternative microfabrication approach utilizes focused ion beam (FIB) implantation as a versatile maskless and resistless process. FIB systems can provide an ion beam with a diameter ranging from a few μm to 100 nm or less. Several FIB techniques can be utilized for this purpose: direct micromachining, maskless lithography, or implantation. The implantation approach accomplishes a certain functional aspect (usually charge carrier or photon confinement) of the device structure through the introduction of ions in order to provide either localized doping or ion-induced compositional mixing of multilayer structures. In addition to the advantages of a high resolution maskless/resistless process, the FIB approach benefits from being able to readily adjust the implantation conditions (such as dose, energy, sometimes even species) in order to customize the process for each type of component during a single step.

FIB techniques have been used to fabricate several types of GaAs-based photonic and optoelectronic devices. Table I contains representative examples from each FIB approach, along with the relevant references.[2–10] The examples range from mirrors fabricated by micromachining, to channel waveguides fabricated by mixing, to laser gratings fabricated by either doping, lithography, or mixing. A broad review of FIB techniques for optoelectronics has recently been published by Harriott and Temkin.[11] In this article, we present a review of our work on the fabrication of optoelectronic components using the FIB-implantation mixing approach.

In most of the work reported in this article, we have used the basic superlattice/quantum well (SL/QW) structure shown in Fig. 1. A (100) GaAs wafer is used as a substrate for an $Al_xGa_{1-x}As$ cladding layer of 1 μm thickness, a 30 nm GaAs QW, a ~200 nm GaAs/$Al_xGa_{1-x}As$ SL with 3.5 nm individual layers, and a 50 nm $Al_xGa_{1-x}As$ cap layer. Wherever present, the relative Al composition was approximately 30%. Implantations were performed with a 150 kV FIB system. The implantation pattern shown as an example in Fig. 1 provides the localized mixing specifically required for the fabrication of a distributed Bragg reflection (DBR) laser: the DBR gratings and the lateral optical confinement. However, the latter is also representative of the pattern used for channel waveguide fabrication. For the study of the mixing process large square regions of several hundred micrometers were uniformly FIB implanted.

II. FIB IMPLANTATION MIXING PROCESS

Laidig *et al.* first reported[12] in 1980 that the individual layers in a GaAs–AlAs SL are converted to a homogeneous AlGaAs material by Zn diffusion at temperatures much below those necessary for ordinary thermal interdiffusion of the undoped SL. In the mixed region, an alloy of average composition is formed with corresponding material properties, including band gap energy and refractive index. By spatially defining the mixing process (with either diffusion or implantation of one of several impurities), effective local confinement of charge carriers and photons can be achieved. Subsequently, the phenomenon has been shown to be more general and mixing through the introduction of other species such as Si, Al, and Ga has also been reported.[13] This has served as the basis for fabricating many important heterojunction and optoelectronic devices.

[a]Electronic-mail: a.steckl@uc.edu

TABLE I. FIB fabricated optoelectronic components.

Component	Application	Fabrication technique	Material system	Reference
Facet reflectors	Vertical emission from horizontal laser cavity	Micromachining	InGaAsP/InP	2
Beam splitters	Ridge channel waveguide	Micromachining	GaAs/AlGaAs	3
Turning mirrors	DBR surface emitting ring laser	Micromachining	GaAs/AlGaAs	4
Buried waveguide	Laser cavity confinement	Mixing (suppression)	GaAs/AlGaAs	5
Channel waveguides	Optical switch, modulator	Mixing	GaAs/AlGaAs	6
Gratings	DBR laser	Doping	GaAs/AlGaAs	7
Gratings+waveguide	DBR laser	Mixing	GaAs/AlGaAs	8
Gratings	DFB laser	Doping (damage)	InGaAs/AlGaAs	9
Gratings	DBR laser	Lithography	InGaAs/GaAs	10

FIB implantation technology is especially attractive for this application, since it provides a maskless process with high spatial resolution. In addition to optimization in the lateral direction, depth control of the mixed region in the vertical direction is also critical for a number of applications. Therefore a solid understanding of the mixing mechanisms is essential for precise control of the mixing process and the fabrication of devices with optimum characteristics.

Our FIB mixing experiments, described in greater detail elsewhere,[14] used on-axis Si^{++} implantation at 100 and 200 keV. This was followed by rapid thermal annealing (RTA) at 950 °C for 10 s, with proximity protection in a forming gas (96% N_2/4% H_2) atmosphere. For a FIB dose of 1×10^{14} cm^{-2}, this condition was verified[15] to be sufficient for localized mixing in the implanted region, while preserving the original SL structure in the unimplanted region. The depth profiles of the Al and Si distributions were precisely measured with secondary ion mass spectroscopy (SIMS).

Intermixing of Al-rich and Ga-rich layers in a SL structure results from Ga–Al interdiffusion during the thermal process. The interdiffusion of column III atoms proceeds primarily through point defects of the crystal. Therefore, the introduction of dopant impurities and excess vacancies will enhance the interdiffusion and, in turn, the intermixing. Very efficient SL mixing has been reported for broad beam ion implantation using Si.[16] The specific mechanisms responsible for intermixing depend on the time frame of the thermal process. Using furnace annealing (FA) for a period of one or more hours results in significant diffusion of the Si impurities. From a device fabrication point of view FA is not desirable since it causes relatively large changes in the lateral profile of the structure, thus limiting the minimum dimensions which can be achieved. By comparison, RTA also yields efficient intermixing while providing a quick, simple, and localized process. In this case, impurity diffusion is not likely to be the dominant mixing mechanism, since in the RTA time scale impurities do not move appreciably.[17,18] Furthermore, in certain cases it has been observed that the maximum intermixing produced by RTA does not occur at the

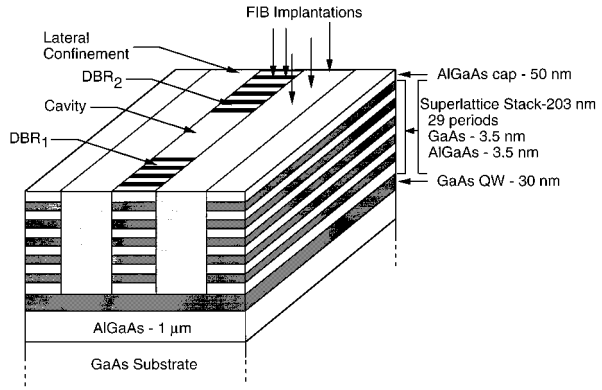

FIG. 1. Cross section of structure used in FIB mixing study and for DBR laser fabrication: GaAs/AlGaAs superlattice with 7 nm period and 30 nm GaAs quantum well. AlAs composition: 0.3. (Ref. 14.)

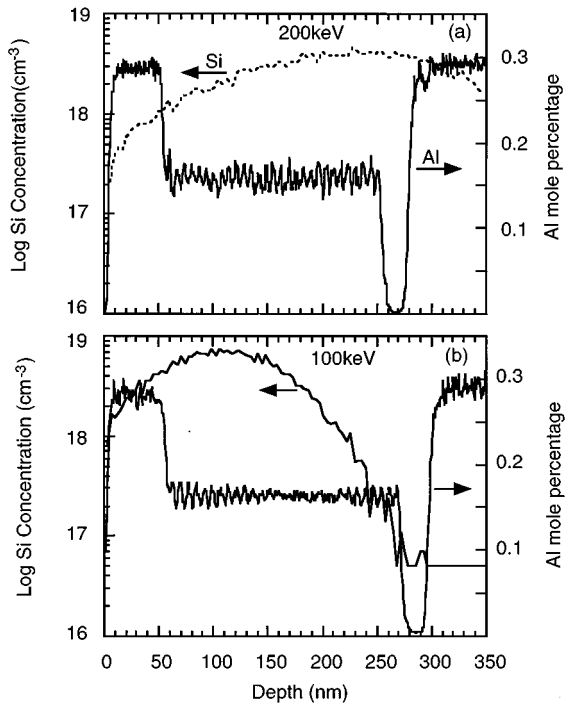

FIG. 2. Si and Al depth profiles of annealed superlattice produced by Si FIB implantation with a 1×10^{14} cm^{-2} dose at energy of (a) 200 keV; (b) 100 keV. (Ref. 14.)

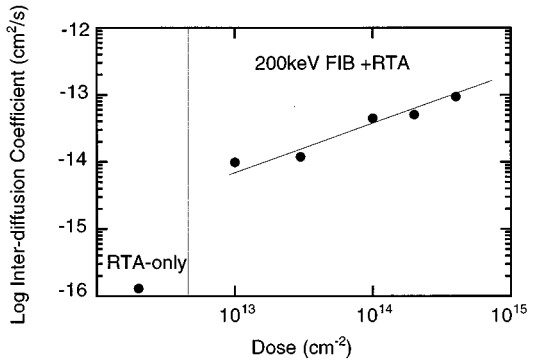

FIG. 3. Al–Ga interdiffusion coefficient as a function of dose for 200 keV Si FIB implantation and RTA. (Ref. 14.)

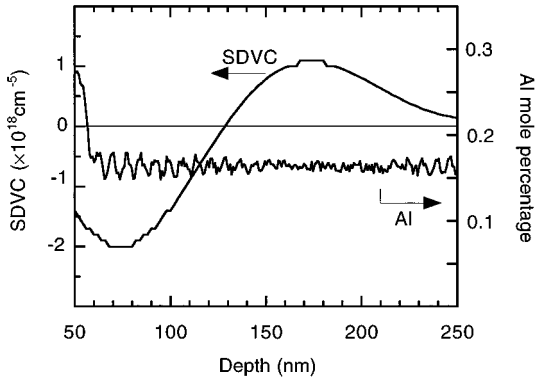

FIG. 5. Depth-dependent mixing in superlattice after 100 keV. Si FIB (1×10^{14} cm^{-2}) implantation and RTA: SDVC and Al depth profiles. (Ref. 14.)

depth corresponding to maximum Si concentration. An interdiffusion model valid within the RTA time frame proposed in Refs. 17–19 attributes the enhancement of interdiffusion to excess vacancies during the transient process rather than to Si diffusion.

Typical Si and Al depth profiles in the SL/QW structure obtained by SIMS after FIB implantation and RTA are shown in Fig. 2. For the 200 keV FIB implantation, uniform mixing of the SL is observed in Fig. 2(a). The Si depth profile peaks deep in the SL, in the vicinity of the QW. Virtually identical Si depth profiles are obtained[14] for the as-implanted and annealed cases, indicating no measurable Si diffusion during RTA. The average interdiffusion coefficient calculated[14] for uniform (200 keV) mixing is a strong function of dose, as shown in Fig. 3. The diffusion coefficient produced by RTA in the absence of implantation was calculated to be $\sim1\times10^{-16}$ cm^2/s, while FIB implantation with a dose of 1×10^{14} cm^{-2} results in a two order of magnitude increase to a diffusivity value of $\sim5\times10^{-14}$ cm^2/s.

For 100 keV ion implantation, the Si profile peaks much closer to the surface. In this case the SL mixing exhibits a ''pinch-off'' region, wherein mixing is much more effective than elsewhere. As shown in Fig. 2(b), the pinch off is peaked in the middle of the SL, below the Si peak concentration. A comparison of the interdiffusion coefficients calculated for 100 and 200 keV FIB implantation is shown in Fig. 4. For 200 keV implantation uniform interdiffusion is obtained as a function of depth. On the other hand, for 100 keV implantation the interdiffusion coefficient in the pinch-off region is 10× larger than that obtained in the rest of the SL structure and approximately 30× larger than the interdiffusion coefficient obtained with 200 keV implantation.

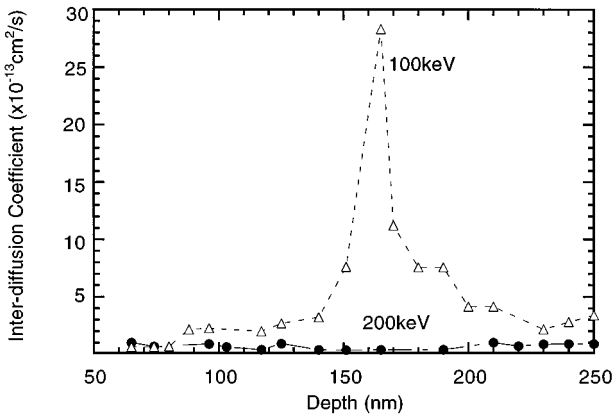

FIG. 4. Al–Ga interdiffusion coefficient as function of depth for Si FIB implantation with dose of 1×10^{14} cm^{-2} at 100 and 200 keV. (Ref. 14.)

Such depth-dependent mixing has been reported,[17–20] but not explained, for various SL structures and processing conditions. We have modified the interdiffusion model in order to accurately predict the mixing depth dependence observed upon FIB/RTA processing. The vacancy and impurity concentrations are clearly still an important factor here because the average degree of mixing over the entire SL is proportional to the dose. However, we have found[14] that in the pinch-off region the mixing is strongly affected by the second derivative of the vacancy concentration (SDVC). The Al concentration after 100 keV FIB/RTA mixing shown in Fig. 2(b) is compared in Fig. 5 to the calculated SDVC depth distribution. The enhanced mixing is observed to occur in the region of large and positive SDVC, with the pinch-off maximum coinciding with the peak SDVC level. We can explain the effect of SDVC on mixing by noting that the SDVC is linearly related to the *time* derivative of the vacancy concentration through Fick's second diffusion law.

Our analysis therefore suggests that the Al–Ga interdiffusion is enhanced by the vacancy injection that takes place in the region where SDVC is positive and sufficiently large. This injection, generated by the presence of a gradient in the transient vacancy concentration (and modified by the recombination of excess vacancies), is presumably responsible for the enhanced mixing occurring in the pinch-off region. Therefore, a section of the SL which has large SDVC will experience rapid vacancy injection upon annealing. Since the vacancy decay time constant is on the order of a few seconds, the SDVC effect is likely to dominate only for RTA.

To obtain high resolution selective-area SL mixing with the FIB-induced approach, one needs to combine reduction of the ion dose (for minimum initial lateral profile) with a reduction in the RTA thermal budget (for minimum lateral outdiffusion). This can be accomplished by a combination of using a short period SL and tailoring the device vertical di-

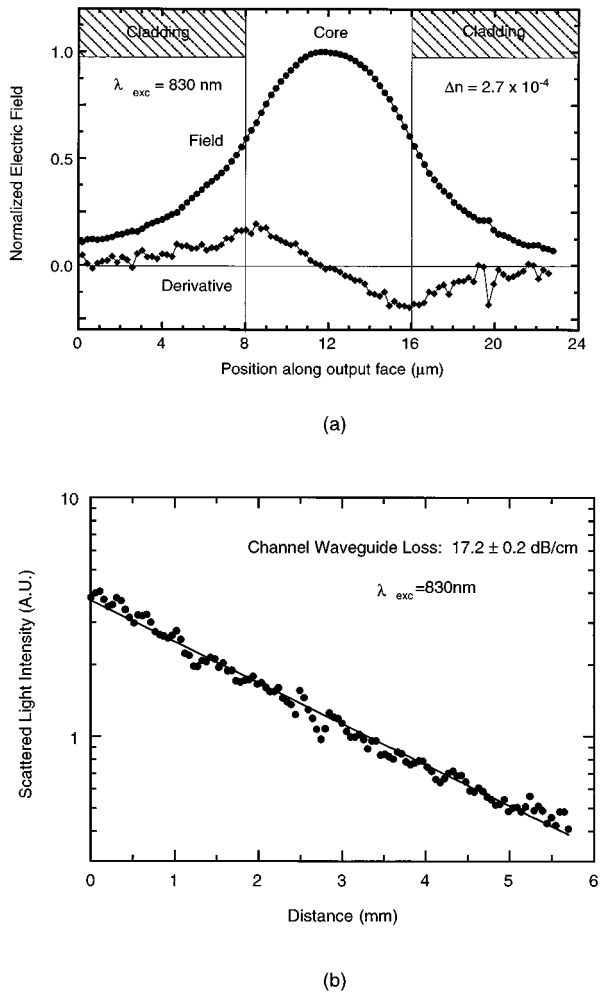

FIG. 6. Channel waveguide fabricated by Si FIB implantation: (a) transverse channel mode light intensity distribution (Ref. 21); (b) normalized outscattered light intensity vs distance along the channel. (Ref. 6.)

mensions such that one can take advantage of enhanced mixing in the pinch-off region.

III. OPTOELECTRONIC COMPONENTS FABRICATED BY FIB MIXING

As indicated in Sec. I, a variety of optoelectronic devices have been implemented with FIB technology. In this section we review two of the most important devices fabricated using FIB mixing of SL and MQW structures: channel waveguides and laser gratings. Channel waveguides formed by FIB-induced compositional mixing are attractive because of the resulting planar structure and the much simplified overall processing. As discussed in Sec. I, FIB processes in general are well suited for optoelectronic integration because of the versatility of the maskless/resistless process which can be applied in process-specific fashion to many of the other components normally required in the circuit.

We have fabricated[6] channel waveguides using an $Al_{0.2}Ga_{0.8}As/Al_{0.13}Ga_{0.87}As$ SL structure designed to support a single mode at a wavelength of 830 nm. The SL stack consisted of 46 periods with 10-nm-thick barrier layers and 5 nm wells for an overall thickness of 700 nm. To obtain channel waveguide operation, two parallel stripes were FIB implanted with 160 keV Si^{++} at a dose of 5×10^{14} cm^{-2}. To produce the actual mixing after FIB implantation, the standard RTA condition of 10 s at 950 °C was utilized. The dimensions of the channel guide were determined by the separation between the stripes (from 4 to 8 μm) and by the length of the stripes ($\sim$1 cm).

Optical waveguiding properties at $\lambda=830$ nm were obtained for end-firing coupling onto a cleaved face of the FIB-mixed sample. The transverse output of the 8 μm channel waveguide[21] is shown in Fig. 6(a) to consist of a single mode with a symmetric profile. The normalized amplitude of the electric field (E field) is calculated from $(I/I_{max})^{1/2}$, where I_{max} is the peak intensity measured along the output face. The spatial derivative of the E field exhibits a peak at the interfaces between the unmixed channel core and the partially mixed cladding regions. The FIB-induced mixing depth can be extracted from the transverse field data using either the magnitude of the E field at the core-cladding interfaces or the evanescent field decay in the cladding regions. In the case of the 8 μm channel shown in Fig. 6(a), a mixing depth range of $\sim$300–325 nm is calculated[20] with the two techniques, representing approximately one-half of the SL stack thickness. Using the latter technique, we also calculate[21] a difference in the effective refractive index between the core and cladding regions of $\sim3\times10^{-4}$.

The intensity loss of the channel waveguide was determined by measuring the outscattered light intensity along the channel length. The normalized scattered light intensity is shown in Fig. 6(b) as a function of propagation distance for the same 8 μm channel guide. The exponential behavior indicates[6] an average loss of $\sim$17 dB/cm, which represents an increased loss of only 5–7 dB/cm over the planar waveguide propagation loss of the structure. The measured value of the channel loss compares favorably with the $\sim$30–60 dB/cm loss reported[22] for channel waveguides fabricated by broad beam implantation. This first demonstration of optical channel waveguiding produced by FIB implantation of a SL structure points to the potential of the FIB mixing technique. Waveguides with channel widths of 1 μm and below are clearly within the capability of FIB technology. Indeed, arrays of parallel confinement regions (''wires'') with $\sim$1 μm individual width have been fabricated by FIB mixing in the SL structure shown in Fig. 1. Anisotropic exciton diffusion, indicating lateral exciton confinement in each wire, was observed[23] by localized photoluminescence in the wire array.

Probably the most significant application of FIB technology for optoelectronic device fabrication involves DBR and distributed feedback (DFB) lasers. DBR and DFB lasers are attractive candidates for light sources in monolithic structures because the absence of cleaved facets allows for direct connection to other optical elements. The DBR laser utilizes two diffraction gratings built into the structure on each side of the active region to provide a high degree of wavelength selectivity, while the DFB approach places the grating above the active region. The fabrication techniques used to fabricate the grating corrugations have combined high resolution (such as holographic, e-beam, or x-ray) lithography and wet chemical etching or ion milling to achieve the submicrome-

ter periods typically required for the GaAs/AlGaAs system. After grating definition, conventional DBR and DFB laser fabrication also necessitate a great deal of process control to complete the device without affecting the grating geometry, including a particularly sensitive second epilayer growth.

On the other hand, FIB technology can deliver the necessary mixing species with a high degree of spatial resolution, given the availability of systems with FIB diameters of ~50–100 nm. In turn, this can produce high resolution gratings through mixing of SL structures in a relatively simple maskless/resistless process. Previous reports of laser structures fabricated by FIB implantation did not employ the direct mixing approach. For example, Ishida *et al.* have fabricated[5] a stripe geometry AlGaAs MQW laser using 40 keV Be^+ FIB implantation in the stripe to *suppress* mixing in the Si-doped MQW. FIB implantation to generate a periodic variation in refractive index due to changes in the free carrier concentration has been utilized by Wu *et al.*[7] to produce a single second-order DBR grating in an AlGaAs/GaAs laser structure. In this case, 100 keV Si^+ FIB implantation with a dose of $\sim 4-8\times10^{14}$ cm^{-2} has been used.

We have utilized the AlGaAs/GaAs structure shown in Fig. 1 for DBR laser fabrication. The QW and SL dimensions were designed such that emission from the active layer will not be absorbed in the grating. The gratings in the two DBR sections each consist of 1000 equally spaced lines. The grating period was chosen to be 350 nm, corresponding to a third-order grating. A 140-μm-long resonant cavity was formed by separating the gratings into two parallel arrays. Lateral confinement within a 25 μm channel waveguide is provided by two 10-μm-wide implanted stripes. FIB-induced mixing was employed for the fabrication of both the gratings and the waveguide.

FIB implantation for gratings and waveguide fabrication was performed with a 200 keV Si^{++} ion beam with a current of 25 pA and a diameter of ~60–70 nm. A dose of 1×10^{14} cm^{-2} (equivalent to a line dose of $\sim1\times10^{8}$ cm^{-1}) was used, which as discussed in Sec. II [see Figs. 2(a) and 3] was found to be sufficient for effective mixing of the SL stack. After implantation, the structure was annealed at 950 °C for 10 s, which are the same conditions previously established for selective mixing and waveguide fabrication (see Sec. II and Ref. 15). It is important to point out that the grating fabrication by FIB-induced mixing was actually obtained at a lower dose than that reported[7] for gratings fabricated by FIB-implanted periodic variations in doping concentration. As discussed in Sec. II, careful design of the laser structure and of the implantation and annealing conditions to take advantage of the enhanced mixing produced by transient vacancy injection in the pinch-off region of the SL stack should produce even lower doses for DBR/DFB grating fabrication.

Lasing operation of the DBR structure was achieved under optical pumping at temperatures from 77 to 125 K. In the output spectrum obtained at 77 K and shown in Fig. 7, laser emission is observed at 827 nm superimposed on a much lower and broad emission from the QW. A broad emission peak from the SL is also observed at ~740 nm. A much higher resolution scan, restricted to the immediate vicinity of the laser wavelength, is shown in the insert contained in Fig. 7. Three main emission modes are observed, with a linewidth of 1.5 and 2 Å and a separation of ~3 Å. The threshold optical (peak) pumping power for lasing is approximately 10 kW/cm^2. This corresponds to a threshold average pumping energy of less than 1 $\mu J/cm^2$.

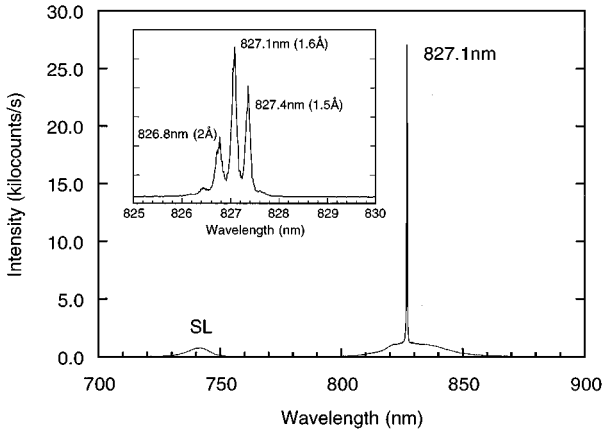

FIG. 7. Photoexcited spectrum emitted from DBR laser structure fabricated by Si FIB implantation: broad PL from SL and QW, and lasing at ~827 nm; inset: high resolution spectrum of 827 nm region. (Ref. 8.)

The DBR coupling coefficient (κ) is a measure of the effectiveness of the grating in providing a high reflectivity. κ for this laser structure has been calculated[8] to be in a range from ~50 to 80 cm^{-1}, which is significantly larger than the value (~15 cm^{-1}) reported[7] for the DBR laser fabricated using FIB-induced carrier concentration modulation. Given that the dose used in our DBR fabrication was also nearly one order of magnitude smaller, this indicates the effectiveness of FIB mixing for laser and other optoelectronic component fabrication. The product of the coupling coefficient and the grating length (κL) determines the maximum grating reflectivity (R_{max}), obtained under phase-matched conditions. For our FIB-fabricated gratings, we calculate a $\kappa L \approx 1.8-2.8$ and an $R_{max} \approx 80\%-90\%$.

Significant new results with FIB implantation for DFB laser fabrication have also been recently reported[9] by Orth *et al.*, using Ga^+ FIB-induced implantation damage to spatially modulate the carrier lifetime in two GaInAs/GaAs QWs.

IV. SUMMARY AND CONCLUSIONS

In this article we have reviewed the salient mechanisms of FIB mixing technology. The technique is very versatile and can clearly be applied to the fabrication of many types of optoelectronic components, including but not limited to the ones discussed here. One of the key issues regarding the eventual wider application of this technology is whether its promise of simpler and more cost-effective integration of multiple components on a single chip is in fact borne out. To date, that has not been attempted. However, the excellent values achieved as first results in channel waveguides, DBR/DFB lasers, and other components encourage us to pursue in the future the FIB fabrication of integrated photonic and optoelectronic circuits.

ACKNOWLEDGMENTS

The authors would like to thank R. Kolbas, S. C. Smith, and R. D. Burnham for the growth of several structures by molecular beam epitaxy and metalorganic chemical vapor deposition, and S. Novak for SIMS measurement and interpretation. The partial support for this work from the National Science Foundation and the Materials Directorate, Wright Laboratory at the Wright–Patterson Air Force Base, is acknowledged.

[1]For various fabrication issues in laser, OEIC, and PIC fabrication see *Integrated Optoelectronics*, edited by M. Dagenais, R. F. Leheny, and J. Crow (Academic, New York, 1994), Chaps. 8, 10, 12, and 15.
[2]L. R. Harriott, R. E. Scotti, K. D. Cummings, and A. F. Ambrose, Appl. Phys. Lett. **48**, 1704 (1986).
[3]J. S. Osinski, C. E. Zah, R. Bhat, R. J. Contolini, E. D. Beebe, T. P. Lee, K. D. Cummings, and L. R. Harriott, Electron. Lett. **23**, 1156 (1987).
[4]D. J. Bossert *et al.*, Appl. Phys. Lett. **56**, 2068 (1990).
[5]K. Ishida, K. Matsui, T. Fukunaga, T. Takamori, and H. Nakashima, Jpn. J. Appl. Phys. **25**, L783 (1986).
[6]M. Kumar *et al.*, IEEE Photon. Technol. Lett. **4**, 435 (1993).
[7]M. W. Wu, M. M. Boenke, S. Wang, W. M. Clark, E. H. Stevens, and M. W. Utlaut, Appl. Phys. Lett. **53**, 265 (1988).
[8]A. J. Steckl, P. Chen, X. Cao, H. E. Jackson, M. Kumar, and J. T. Boyd, Appl. Phys. Lett. **67**, 179 (1995).
[9]A. Orth, J. P. Reithmaier, F. Faller, and A. Forchel, J. Vac. Sci. Technol. B **13**, 2714 (1995).
[10]I. M. Templeton, M. Fallahi, L. E. Erickson, F. Chatenoud, E. S. Koteles, H. G. Champion, and R. Barber, J. Vac. Sci. Technol. B **13**, 2722 (1995).
[11]L. R. Harriott and H. Temkin, in Ref. 1, Chap. 6.
[12]W. D. Laidig, N. Holonyak, Jr., M. D. Camras, K. Hess, J. J. Coleman, P. D. Dapkus, and J. Bardeen, Appl. Phys. Lett. **38**, 776 (1981).
[13]For a review see D. G. Deppe and N. Holonyak, Jr., J. Appl. Phys. **64**, R93 (1988).
[14]P. Chen and A. J. Steckl, J. Appl. Phys. **77**, 5616 (1995).
[15]A. J. Steckl, P. Chen, A. Choo, H. E. Jackson, J. T. Boyd, P. Pronko, A. Ezis, and R. Kolbas, Mater. Res. Soc. Symp. Proc. **240**, 703 (1992).
[16]T. Y. Tan, U. Gösele, and S. Yu, Critical Rev. Solid State Mater. Sci., **17**, 47 (1991).
[17]K. B. Kahen, G. Rajeswaran, and S. T. Lee, Appl. Phys. Lett. **53**, 1635 (1988).
[18]K. B. Kahen and G. Rajeswaran, J. Appl. Phys. **66**, 545 (1989).
[19]S. T. Lee, G. Braunstein, P. Fellinger, K. B. Kahen, and G. Rajeswaran, Appl. Phys. Lett. **53**, 2531 (1988).
[20]S. A. Schwarz, T. Venkatesan, R. Bhat, M. Koza, H. W. Yoon, Y. Arakawa, and P. Mei, Mater. Res. Soc. Symp. Proc. **56**, 321 (1986).
[21]M. Kumar, A. G. Choo, P. Chen, G. N. De Brabander, J. T. Boyd, H. E. Jackson, A. J. Steckl, R. D. Burnham, and S. C. Smith, Superlatt. Microstruct. **15**, 421 (1994).
[22]B. L. Weiss, A. C. Wismayer, and J. Roberts, Electron. Lett. **25**, 653 (1989).
[23]A. Choo, X. Cao, S. Tlali, H. E. Jackson, P. Chen, A. J. Steckl, and J. T. Boyd, Mater. Res. Soc. Symp. Proc. **324**, 193 (1994).